Available online at www.sciencedirect.com
ScienceDirect
Journal of Sound and Vibration 317 (2008) 354–365
JOURNAL OF SOUND AND VIBRATION
www.elsevier.com/locate/jsvi

Perfectly matched layers for modelling seismic oceanography experiments

Jean Kormann[a], Pedro Cobo[a,*], Andrés Prieto[b]

[a]*Instituto de Acústica, CSIC, Serrano 144, 28006 Madrid, Spain*
[b]*Departamento de Matemática Aplicada, Universidad de Santiago de Compostela, 15782 Santiago de Compostela, Spain*

Received 23 October 2007; received in revised form 13 March 2008; accepted 17 March 2008
Handling Editor: C.L. Morfey
Available online 2 May 2008

Abstract

Seismic oceanography techniques are able to provide oceanographic properties of the water masses by processing seismic reflection data. These techniques have reported reflected waves due to the fine structure in the ocean, whose order of magnitude is as weak as −80 dB. Thus, if we focus our attention on numerical simulation of this kind of oceanography experiments, the numerical performance of the method should allow obtaining accurate results, where the spurious reflections from the artificial boundaries of the computational grid are, at least, one order of magnitude smaller than the physical phenomena. This can be achieved by introducing perfectly matched layers (PML), which simulate non-reflecting boundaries. The aim of this work is to propose a numerical underwater propagation method, which combines a second-order finite-difference scheme in the physical region of interest with a first-order pressure/velocity discretization in the PML domain. This numerical method provides a low-cost computational algorithm with an accuracy, which allows recovering the reflected phenomena from the ocean fine structure, and moreover, with a spurious error of order −100 dB from the PML domain.
© 2008 Elsevier Ltd. All rights reserved.

1. Introduction

Most of the regions of the ocean contain water masses with different temperature and salinity characteristics, which produce a relative motion among them. In fact, there exists a thermohaline fine-scale structure and thermohaline intrusions in the interfaces between these water masses. Both structures are important manifestations of mixing processes in the ocean [1]. These mechanisms, which transport heat from the equator toward the poles, cooling the tropics and warming higher latitudes, conform the climate machine of the ocean [2].

Fine structure in the ocean can be mapped by oceanographic probes that measure depth profiles of temperature and salinity. Such techniques have practical limitations for achieving an accurate lateral resolution due to the small ocean volume that can be imaged. Holbrook et al. [1] presented evidence that the

*Corresponding author. Tel.: +34 91 5618806; fax: +34 91 4117651.
E-mail address: pcobo@ia.cetef.csic.es (P. Cobo).

0022-460X/$ - see front matter © 2008 Elsevier Ltd. All rights reserved.
doi:10.1016/j.jsv.2008.03.024

oceanic fine structure can be mapped with a high lateral resolution using standard seismic reflection techniques. Typically, marine seismic sources have a spectral content below 110 Hz. Thus, acoustic waves propagated in the water mass have a vertical resolving power of several metres. Long streamers of hydrophones of several kilometres are capable of mapping large ocean regions, with a lateral resolution of order of the acoustic wavelength (typically 20–30 m). Holbrook and Fer [3] suggested the term *seismic oceanography* for the seismic reflection techniques applied to retrieve oceanographic properties of the water masses in the ocean.

The contact surface between distinct water masses produces acoustic impedance contrasts. Although the reflected wave phenomena in such regions are weak, the large amount of energy raised by a seismic source can generate measurable reflected energy in the hydrophones. Holbrook et al. [1] measured scattered waves, whose magnitude was as weak as -80 dB. These measures corresponded to sound speed changes of 0.3 m/s (temperature variation of 0.1 °C), in a marine seismic reflection cruise across the oceanographic front between the Labrador Current and the North Atlantic Current.

Seismic oceanography experiments can be simulated numerically by using standard underwater acoustic propagation algorithms (see, for instance, [4]) and considering physical data for the boundary conditions at the surface and bottom oceanic interfaces. However, since the ocean is unbounded along the lateral spatial coordinate, then artificial boundaries must be introduced at both lateral sides of the physical domain of interest. This truncation allows to bound the computational domain in the numerical simulations but, at the same time, it should not introduce numerical spurious reflections in the physical region. Among other methods, two kinds of numerical techniques can be used to truncate the unbounded physical domain of wave propagation: the absorbing boundary conditions (ABC) and the perfectly matched layers (PML). Local ABCs were introduced by Engquist and Majda [5] and subsequently improved from a computational point of view by different authors [6]. More recently, Berenger [7] introduced an alternative approach to deal with the truncation of unbounded domains based on simulating an absorbing layer of anisotropic material which matches perfectly with the physical domain of interest, and thus, avoids spurious reflections from the lateral boundaries. Although the PML method was introduced originally for electromagnetic waves, it has been further extended to model elastic [8] and acoustic waves [9]. More specifically, Liu and Tao [10] used the PML method with underwater acoustic propagation models.

In conclusion, if we focus our attention on the numerical simulation of the seismic oceanography experiments with an oceanic fine structure, then the magnitude of the reflected waves at the truncating lateral boundaries plays a more relevant role than in other physical wave propagation problems. Since the fine structure yields weak reflected waves, spurious numerical reflections at the lateral PML boundaries must be at least one order smaller than the magnitude of the physical phenomena of interest. The main goal of this work is to describe an accurate and low-cost numerical method, which combines the PML technique with two different coupled finite-difference schemes, in the framework of oceanography experiments with a fine structure.

The outline of this paper is as follows: in Section 2 we describe the proposed numerical algorithm. For the sake of completeness in the exposition, in Section 2.1 we derive briefly the wave equation in the physical region. The two finite-difference schemes used for the physical and PML domain are explained in Sections 2.2 and 2.3, respectively. The combination of the chosen finite-difference schemes and the PML technique with singular coefficients leads to a reduction of the time computation and memory storage and increases the global precision of the numerical simulations for seismic oceanography experiments. The numerical accuracy of the proposed method is illustrated in Section 3 by comparing the traces received at three depths with reference traces and with those provided by the first-order method proposed by Liu and Tao [10]. The reference traces are obtained by doubling the dimensions of the physical region, so that no reflected waves in the PML reach the receivers. Moreover, we show some numerical results that illustrate the performance of the proposed algorithm with a realistic sound-speed profile.

2. Description of the propagation algorithm

In this section, we present a combined algorithm where an explicit second-order finite-difference scheme for the physical domain is matched with an explicit first-order pressure/velocity discretization in the PML region.

2.1. Statement of the model

In this subsection, we develop the equations involved in the model of the underwater wave propagation in the Lagrangian description [11].

Firstly, in the framework of the standard assumptions in linear acoustics where the thermodynamic process is isentropic, i.e., if we assume that the entropy is preserved constant with respect to the time, the energy and motion equation of an isentropic compressible fluid can be written in terms of the pressure fluctuation p and the velocity $\mathbf{v}$, which satisfies the governing equations

$$\rho \frac{\partial \mathbf{v}}{\partial t} = -\nabla p, \tag{1}$$

$$\frac{\partial p}{\partial t} = -\rho c^2 \operatorname{div} \mathbf{v}, \tag{2}$$

ρ and c being, respectively, the mass density and the sound speed of the fluid in an initial state at rest. Now, deriving with respect to the time in Eq. (2), we have

$$\frac{\partial \mathbf{v}}{\partial t} = -\frac{1}{\rho} \nabla p, \tag{3}$$

$$\frac{\partial^2 p}{\partial t^2} = -\rho c^2 \operatorname{div} \frac{\partial \mathbf{v}}{\partial t}. \tag{4}$$

Finally, introducing Eq. (3) into Eq. (4) provides

$$\frac{\partial^2 p}{\partial t^2} - \rho c^2 \operatorname{div}\left(\frac{1}{\rho} \nabla p\right) = 0, \tag{5}$$

which is the so-called Pekeris' equation. Let us remark that both fields ρ and c are not assumed to be constant in the previous equation. Obviously, if the mass density is constant then the above equation is reduced to the wave equation

$$\frac{\partial^2 p}{\partial t^2} - c^2 \operatorname{div}(\nabla p) = 0. \tag{6}$$

Let us remark that assuming ρ to be constant does not mean neglecting completely small density variations along the water column. Smooth changes of the mass density can still be included in the sound velocity profile through

$$c = \sqrt{\frac{K}{\rho}}, \tag{7}$$

where K is the compression modulus of the fluid [12]. Therefore, in the following we will assume that the simpler Eq. (6) governs the wave propagation in the physical domain. This, in turn, allows us to take advantage of the Laplacian discretization which is second-order in space.

2.2. Finite-difference scheme in the physical region

As mentioned above, the main difficulty of simulating numerically the seismic oceanography experiments consists of the high accuracy required for computing the weak reflections coming from the oceanic fine structure. In this context, although the explicit first-order finite-difference schemes which discretize the system of Eqs. (1) and (2) are low-cost computationally, they provide a precision of order $O(\Delta t)$ in the pressure field due to the computation only of it's first time derivative. Hence, to compute an accurate acoustic scattered field, it would be necessary to decrease the time step and consequently, to increase the computational cost of the algorithm.

However, since we only focus our attention on the spurious reflection from the PML region and not on computing an accurate pressure field inside the PML region, we can combine a second-order propagation algorithm, to take advantage of the $O(\Delta t^2)$ precision in the propagating medium, and use only a explicit first-order finite-difference scheme in the PML region for the standard first-order PML formulation in terms of the pressure and velocity field.

In the following we describe briefly the propagation algorithm in the physical region for the wave equation, which consists of a finite-difference scheme implemented on a uniform grid with the same size Δ in the x- and z-axis. For a given discrete field φ, we denote by $\varphi^n_{\alpha\beta}$ the nodal value of the field at the grid point $(\alpha\Delta,\beta\Delta)$ and at time step $n\,\Delta t$. Therefore, the classical explicit second-order finite-difference scheme for Eq. (6) yields

$$\frac{1}{c_{ij}^2}\frac{p_{ij}^{n+1}-2p_{ij}^n+p_{ij}^{n-1}}{\Delta t^2}=\frac{p_{ij+1}^n-2p_{ij}^n+p_{ij-1}^n}{\Delta^2}+\frac{p_{i+1j}^n-2p_{ij}^n+p_{i-1j}^n}{\Delta^2}. \tag{8}$$

2.3. PML model

For the sake of completeness in the exposition, the derivation of the Berenger PML model using the splitting rule is detailed in the following. Let us start with the Fourier transform of the motion and mass conservation equations expressed in terms of the velocity and pressure fields. Following Chew and Weedon [13], a complex coordinate stretching is introduced by defining a new variable, $\hat{\eta}$, for each spatial variable $\eta = x,z$

$$\hat{\eta}=\eta+\frac{\mathrm{i}}{\omega}\int_{\eta_0}^{\eta}\sigma_\eta\,\mathrm{d}\eta', \tag{9}$$

where σ_η is the so-called absorbing function in the η-direction. Now, formally replacing the derivatives of η by the derivatives of the new complex variable $\hat{\eta}$, it yields

$$\begin{aligned}-\mathrm{i}\omega\rho V_\eta&=-\frac{1}{1+\mathrm{i}(\sigma_\eta/\omega)}\frac{\partial P}{\partial\eta},\\ -\mathrm{i}\omega P&=-\rho c^2\sum_{\eta=x,z}\frac{1}{1+\mathrm{i}(\sigma_\eta/\omega)}\frac{\partial V_\eta}{\partial\eta},\end{aligned} \tag{10}$$

where V_η is the Fourier transform of the η-component of the particle velocity. Following the original idea developed by Berenger [7], the next step consists of introducing the split pressure variables in Eq. (10). It yields the coupled first-order PML equations in the frequency domain

$$\begin{aligned}(-\mathrm{i}\omega+\sigma_\eta)\rho V_\eta&=-\frac{\partial P}{\partial\eta},\\ (-\mathrm{i}\omega+\sigma_\eta)P^{(\eta)}&=-\rho c^2\frac{\partial V_\eta}{\partial\eta},\end{aligned} \tag{11}$$

where $P^{(\eta)}$ are the Fourier transforms of the split pressure variables. The inverse Fourier transform of Eq. (11) can be solved numerically with the following first-order finite-difference scheme:

$$\rho\left(\frac{v_{x,i+j/2}^{n+1/2}-v_{x,i+j/2}^{n-1/2}}{\Delta t}+\frac{\sigma_{x,i+j/2}}{2}\left(v_{x,i+j/2}^{n+1/2}+v_{x,i+j/2}^{n-1/2}\right)\right)=-\frac{p_{i+1j}^n-p_{ij}^n}{\Delta}, \tag{12}$$

$$\rho\left(\frac{v_{z,ij+1/2}^{n+1/2}-v_{z,ij+1/2}^{n-1/2}}{\Delta t}+\frac{\sigma_{z,ij+1/2}}{2}\left(v_{z,ij+1/2}^{n+1/2}+v_{z,ij+1/2}^{n-1/2}\right)\right)=-\frac{p_{ij+1}^n-p_{ij}^n}{\Delta}, \tag{13}$$

$$\frac{p_{ij}^{(x),n+1}-p_{ij}^{(x),n}}{\Delta t}+\frac{\sigma_{x,i+j/2}}{2}\left(p_{ij}^{(x),n+1}+p_{ij}^{(x),n}\right)=-\frac{\rho c_{ij}^2}{\Delta}\left(v_{x,i+j/2}^{n+1/2}-v_{x,i-j/2}^{n+1/2}\right), \tag{14}$$

$$\frac{p_{ij}^{(z),n+1}-p_{ij}^{(z),n}}{\Delta t}+\frac{\sigma_{z,ij+1/2}}{2}\left(p_{ij}^{(z),n+1}+p_{ij}^{(z),n}\right)=-\frac{\rho c_{ij}^2}{\Delta}\left(v_{z,ij+1/2}^{n+1/2}-v_{z,ij-1/2}^{n+1/2}\right), \tag{15}$$

where $p_{ij}^{(x),n}$ and $p_{ij}^{(z),n}$ are the nodal values of the split pressure field $p^{(x)}$ and $p^{(z)}$, respectively.

The final step in the construction of the propagation algorithm consists of introducing the combination between the finite-difference schemes for the physical and PML domain. To match adequately the discrete equations in the physical and PML domain, we impose the continuity of the pressure field. Moreover, the velocity field on the interface between both regions must be re-computed by using Eqs. (12) and (13) with the nodal pressure values close to the interface between the physical and the PML domains.

Let us remark that, instead of the previous first-order PML Berenger formulation, other authors have already used second-order formulations with the split pressure variables. Some of them demonstrated the efficiency of the PML formulation for solving underwater problems in the frequency domain [14–16]. Komatitsch and Tromp [17] presented a second-order algorithm in the time domain for elastic propagation but it was more expensive in terms of memory storage. However, to the author's knowledge, there does not exist a second-order formulation that directly solves the acoustical time-domain problem with a PML system in the Berenger formulation with a unique pressure field. Instead of these alternative formulations, our numerical approach provides a second-order algorithm in time for the pressure field in the propagation domain, which enhances the exactitude of the solution without increasing appreciably the computational cost and the memory storage. As an example, Table 1 compares the computation times of our mixed algorithm with the first-order splitted algorithm proposed by Liu and Tao [10], in (200×200) and (400×400) grids for 1500 iterations (computation carried out with a 64-bit AMD processor and 2 Go ram). The time computation is decreased by 15% in both cases.

3. Numerical results

This section presents two numerical simulations of underwater acoustic propagation using the algorithm described in Section 2.

3.1. PML efficiency analysis

In this first numerical simulation, we focus our attention on comparing the numerical performance of this method with two different implementations and with two different profiles for the absorbing function in the PML domain: the classical PML implementation of Liu and Tao [10] and our propagation algorithm with the exact PML approach proposed by Bermudez et al. [18].

In this numerical example, we consider a non-dissipative isotropic medium with a constant density set to $1000\,\mathrm{kg/m^3}$ and a constant sound velocity equal to 1500 m/s. The PML thickness is set to 100 m, and the source is a spatial monopole multiplied by a Ricker wavelet

$$h(t)=\left[1-2\pi^2 f_0^2(t-t_0)^2\right]\mathrm{e}^{-\pi^2 f_0^2(t-t_0)^2}, \tag{16}$$

where f_0 is the central frequency (60 Hz in this example) and t_0 is the time shift of the wavelet. The grid size is set to 1 m to avoid numerical dispersion, and the time step is set to 0.4 ms, unless specified.

Fig. 1 shows a sketch of the medium where the numerical implementation described above will be compared with that of Liu and Tao [10]. The source is placed at mid-range, 5 m deep. The region is 400 m deep and 100 m

Table 1
Computation times of the first-order and mixed algorithms for 1500 iterations in a grid with (200×200) and (400×400) points

Algorithm	Computation time (s)	
	(200×200)	(400×400)
First-order [10]	75	225
Mixed	63	193

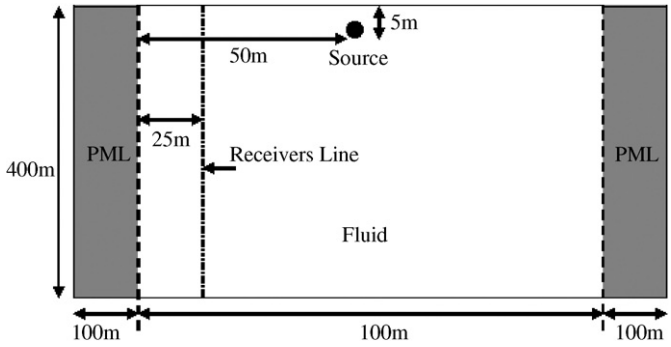

Fig. 1. Sketch of the medium/PML domain with the positions of the source and the receivers.

long. There are two PML zones, on the lateral sides of the physical region. The receivers are located vertically at 25 m from the left medium/PML interface. The σ_η function is the non-integrable hyperbolic one, similar to those proposed by Bermudez et al. [18]

$$\sigma_\eta = 2c\left(\frac{1}{\eta^{\mathrm{T}} - \eta_0} - \frac{1}{\eta^{\mathrm{T}} - \eta}\right), \quad \eta = x, z, \tag{17}$$

where $\eta^{\mathrm{T}} - \eta_0$ is the thickness of the PML layers. This σ_η function presents some advantages as compared to the classical quadratic one. First, from a theoretical point of view, it is possible to prove that, if the mass density and sound speed are constant, then the solution of the original wave propagation problem is exactly recovered by using the PML technique. Second, from a computational point of view, we achieve a better numerical performance than in the case of the bounded absorbing functions. Moreover, in the frequency domain, optimal numerical results are obtained independently of the grid size and the data of the problem [18].

Fig. 2 shows the synthetic traces provided by the mixed and first-order [10] formulations, as compared to the reference trace, at the receivers located at depths of 5, 50 and 100 m. The reference solution is obtained by doubling the medium dimensions, such that there are no reflected waves on the synthetic trace. All the traces are normalized by the maximum of the reference one. Fig. 2(a) shows the results for the first-order (Liu) formulation and Fig. 2(b) for the mixed formulation. At the resolution of the figure, no differences can be seen between both traces.

Fig. 3 shows the error between the reference and the traces provided by the Liu and mixed formulations. Due to the above-described normalization procedure, the error represents the amplitude of the reflected wave at the receiver location. It is clear that the mixed formulation provides less error than the first-order formulation. For instance, at the receiver 100 m deep, the error for the first-order PML is twice that of the mixed formulation. Note that the reflections from the mixed formulation are smaller than 0.0001 (−80 dB), as expected.

In order to compare the numerical performance of different σ_η absorbing functions, let us consider the signals recorded at four receivers on the line depicted in Fig. 4. Two σ_η functions are considered: one is the non-integrable function defined by Eq. (17) and the other one is the classical quadratic function

$$\sigma_\eta = 400\left(\frac{\eta - \eta^0}{\eta^{\mathrm{T}} - \eta^0}\right)^2. \tag{18}$$

In both cases, we use the propagation algorithm described in Section 2 and the PML thickness is set to four wavelengths of the Ricker wavelet. The source is located at the centre of the physical medium. Fig. 5 shows the signal recorded at four different ranges. As can be seen, when the absorbing function is non-integrable, we observe a reflected wave with a smaller amplitude. For instance, in Fig. 5(a), the amplitude of the reflected wave with the quadratic absorbing function is approximately two times larger than the amplitude computed in the non-integrable case.

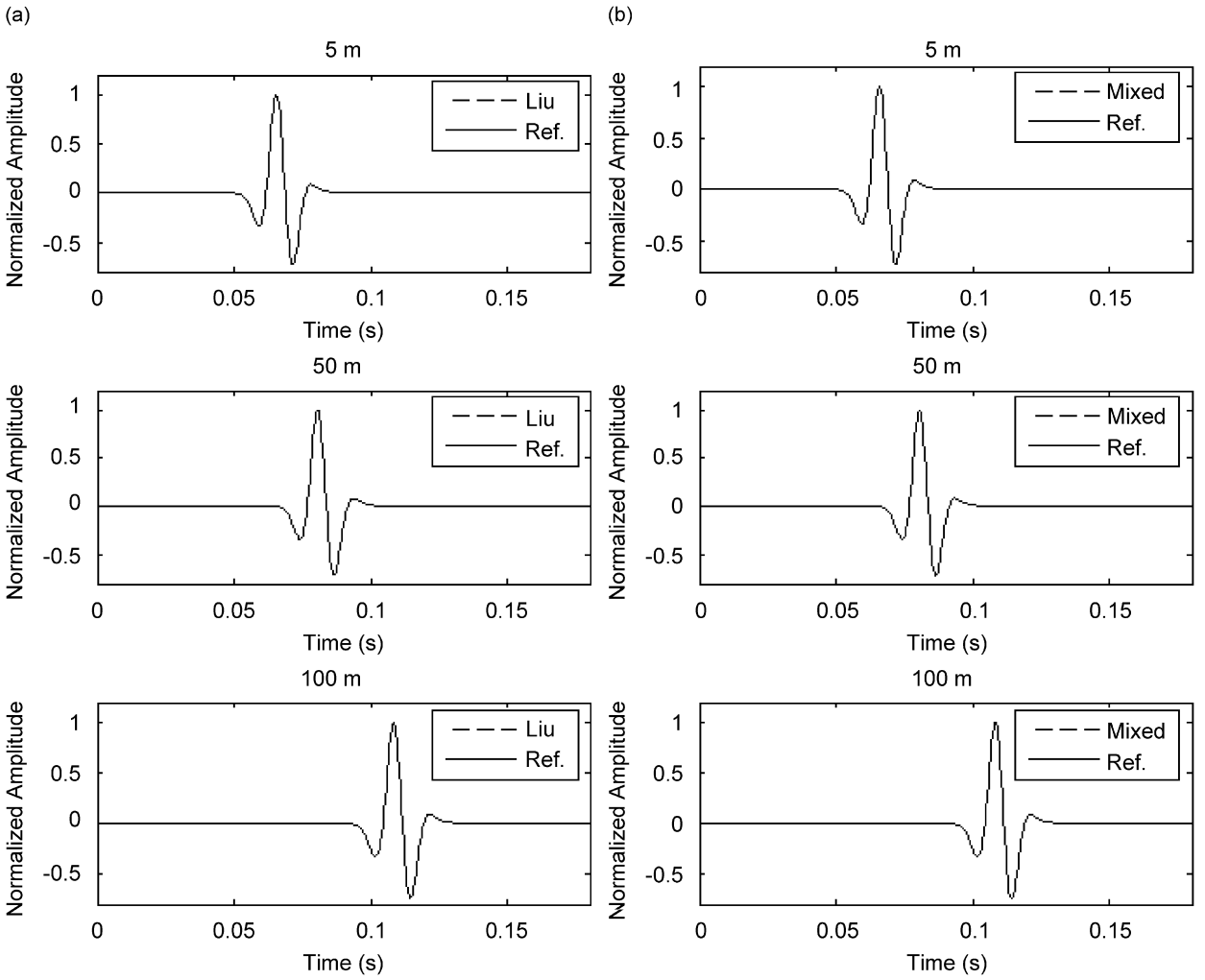

Fig. 2. Traces comparison between the reference solution and that provided by the (a) Liu and (b) mixed formulations at three depths.

3.2. Seismic oceanography experiment

The experiment simulated in Fig. 6 consists of a source and a 2000 m long streamer, both located close to the surface, in a medium with range 2000 m and depth 1000 m. In this numerical simulation the source and the streamer are submerged at 15 and 20 m, respectively, under the sea surface. Three PML regions are placed at both lateral sides and the bottom. The sound-speed field depends on depth only, without lateral variation. The sound-speed profile, which is shown in Fig. 7, is representative of the mixing of Mediterranean and Atlantic water masses in the Gulf of Cadiz (Spain). As we have mentioned in Section 2, small variations in the mass density are unimportant in the physical domain and hence, we assume a constant value of 1000 kg/m^3 in the PML regions. The source is again a spatial monopole multiplied by a Ricker wavelet with a central frequency of 60 Hz. Since we want to observe the numerical reflections on the exterior boundaries of the PML region and, also, on the interface between the physical and PML domain, the total time of simulation is set to 3 s.

Fig. 8(a) shows the shot gather obtained with the above-described data. At the resolution of the figure, no reflected waves can be seen coming from the right and left PML lateral regions. However, the reflection from the bottom PML can be observed at time 1.5 s approximately (marked on the figure). Fig. 8(b) consists of a zoom of the shot gather between 0 and 1.6 s. Again, we only observe the reflections which are coming from the bottom PML region.

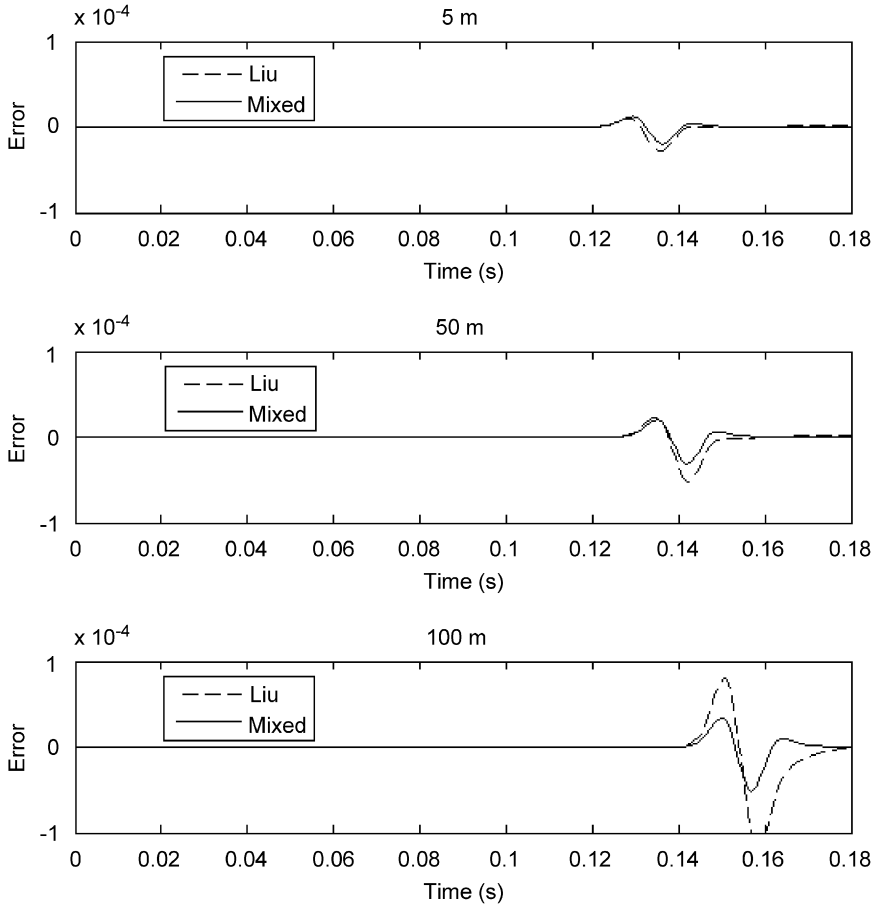

Fig. 3. Comparison of numerical errors between the reference trace and that provided by the Liu and mixed formulations at three depths.

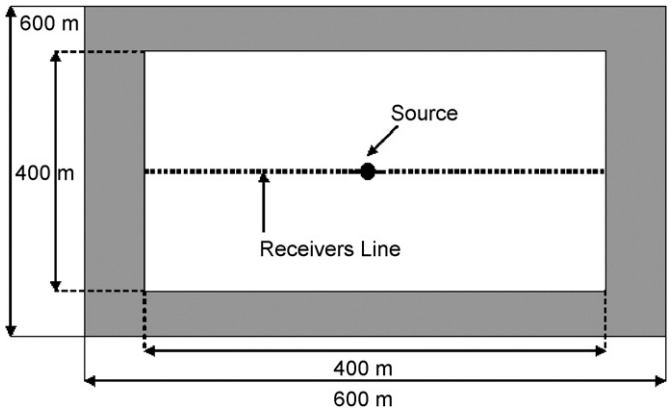

Fig. 4. Sketch of the medium/PML domain for the comparison between the σ_η functions.

In Fig. 9, we plot the trace of the signal recorded in a receiver at 50 m from the source. According to the real-life seismic experiment, a weak scattering due to the small variations of the velocity profile is observed in the trace. Moreover, the amplitude of these weak reflected waves is of order 10^{-4}, as it can be checked more clearly in the zoom around 1.5 s of the entire trace (see Fig. 9(b)). A reflected wave from the bottom PML

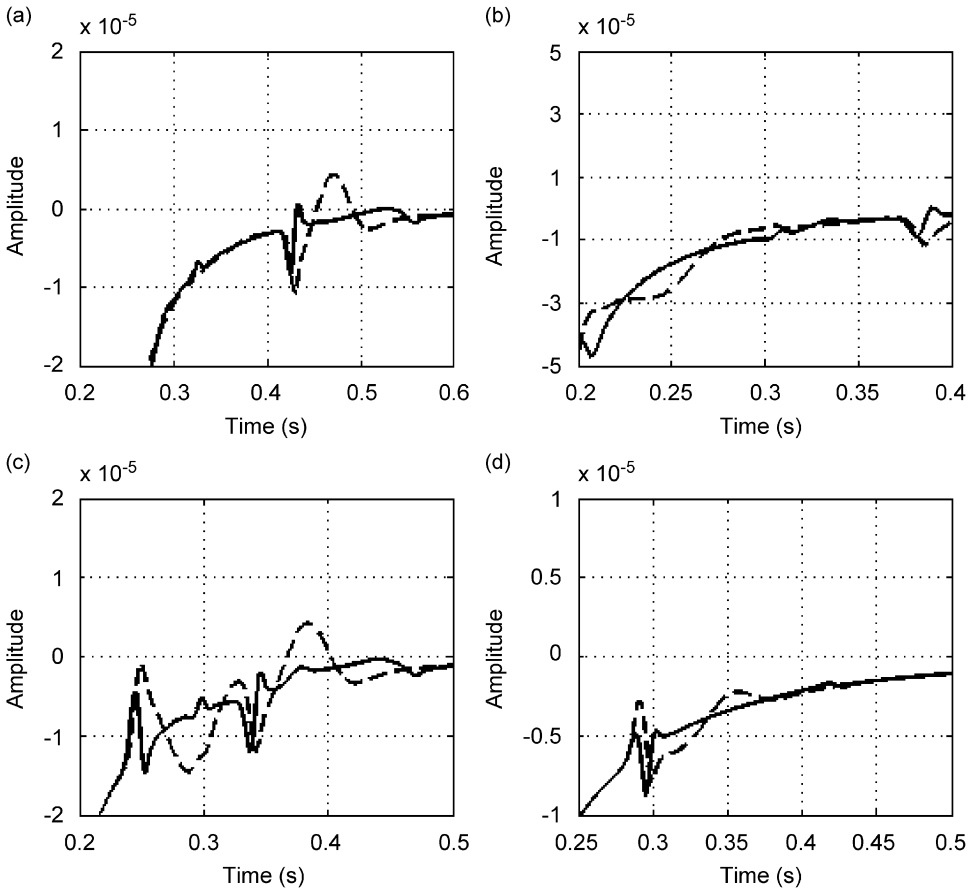

Fig. 5. Zoom on the recorded signals at four ranges along the receivers line for the quadratic (dashed line) and non-integrable (solid line) absorbing functions: (a) 0 m, (b) 54 m, (c) 116 m, and (d) 200 m.

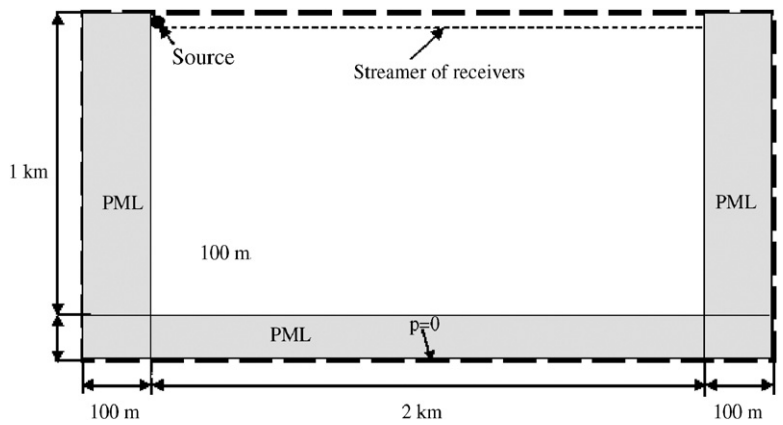

Fig. 6. Sketch of the medium/PML domain for the seismic oceanography experiment simulation.

region at time 1.5 s is also observed in Fig. 9(b). Notice that its amplitude is smaller than those of the scattered waves from the fine structure of the sound-speed profile. A closer zoom of the trace at time larger than 1.5 s is shown in Fig. 9(c). We observe signal amplitudes of order 10^{-7} which correspond to numerical errors from the finite-difference schemes.

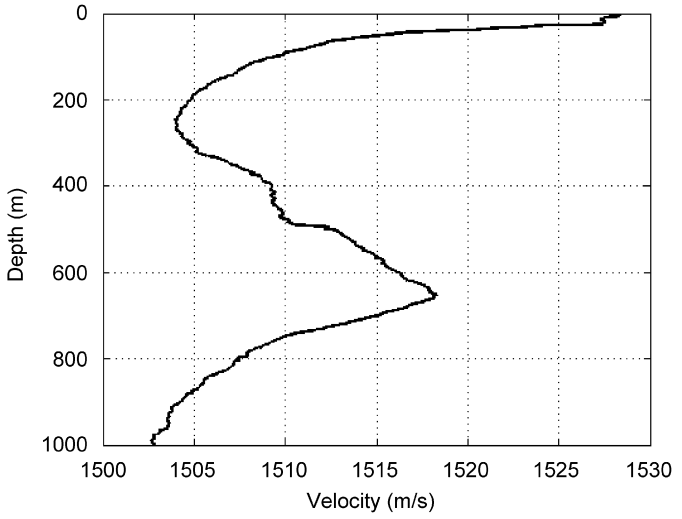

Fig. 7. Sound-speed profile representative of the Mediterranean/Atlantic water mixing in the Gulf of Cadiz.

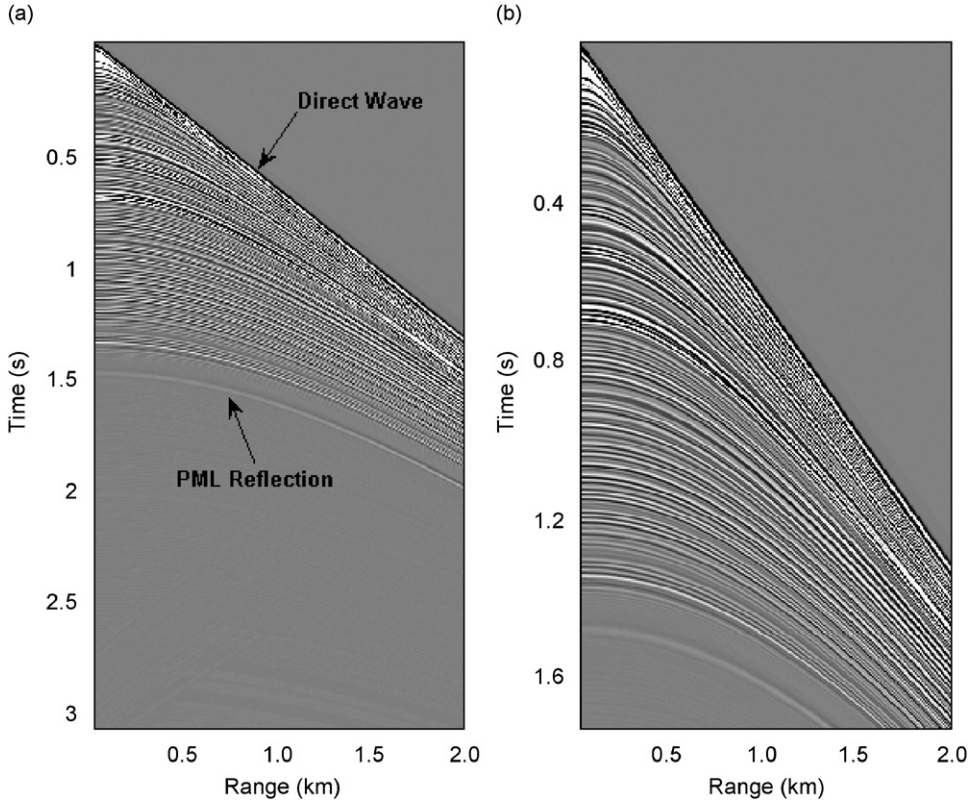

Fig. 8. (a) Synthetic shot gather for the medium/PML sketched in Fig. 6 with the velocity profile of Fig. 7, and (b) a zoom between $t = 0$ s and 1.6 s.

4. Conclusion

We have proposed a numerical algorithm which is able to simulate wave propagation phenomena in seismic oceanography experiments with a weak fine structure. The algorithm uses the PML technique and a

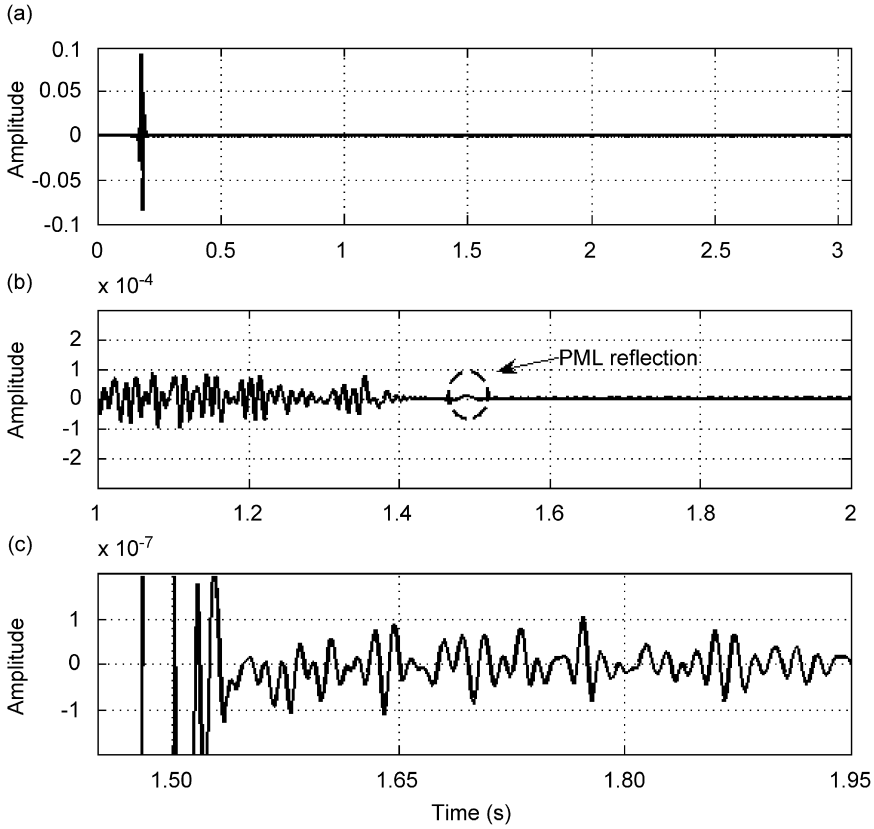

Fig. 9. (a) Synthetic trace at range 50 m, (b) a zoom around the bottom PML reflection ($t = 1.5$ s), and (c) a closer zoom between $t = 1.5$ s and 1.95 s.

combination of low-order finite-difference schemes, for computing *seismic* signals generated by reflections from very low impedance contrast structures in the water column. Because of the low acoustic impedance contrast between typical water column structures, highly accurate techniques for simulating unbounded domains are very relevant. With this purpose, the proposed model includes two lateral PML domains in order to simulate unbounded lateral sides of the physical medium. The propagation algorithm combines a first-order algorithm, based on the PML Berenger formulation with a non-integrable absorbing function, and an explicit second-order finite-difference scheme in the propagation domain. This numerical approach leads to reflections on the interface between the physical medium and the PML of order 10^{-5}. It has been shown that this mixed formulation improves previous results using classical first-order schemes.

Acknowledgments

This work was financially supported partly by the CSIC through Grant No. PIF200530f0081 and partly by the Xunta de Galicia through Grant. No. PGIDIT07PXIB105257PR. The authors are grateful to Valenti Sallares, from the UTM-CMIMA (CSIC), for providing the sound-speed profile.

References

[1] W.S. Holbrook, P. Páramo, S. Pearse, R.W. Schmitt, Thermohaline fine structure in an oceanographic front from seismic reflection profiling, *Science* 301 (2003) 821–824.
[2] B. Ruddick, Sounding out ocean fine structure, *Science* 301 (2003) 772–773.

[3] W.S. Holbrook, I. Fer, Ocean internal wave spectra inferred from seismic reflection transects, *Geophysical Research Letters* 32 (2005) L15604.
[4] F.B. Jensen, W.A. Kuperman, M.B. Porter, H. Schmidt, *Computational Ocean Acoustics*, Springer, New York, 2000.
[5] B. Engquist, A. Majda, Absorbing boundary conditions for the numerical simulation of waves, *Mathematics of Computation* 31 (1977) 629–651.
[6] D. Givoli, T. Hagstrom, I. Patlashenko, Finite element formulation with high order absorbing boundary conditions for time-dependent waves, *Computational Methods in Applied Mechanics* 195 (2006) 3666–3690.
[7] J.P. Berenger, A perfectly matched layer for the absorption of electromagnetic waves, *Journal of Computational Physics* 114 (1994) 185–200.
[8] Q.H. Liu, Perfectly matched layer for elastic waves in cylindrical and spherical coordinates, *Journal of the Acoustical Society of America* 105 (1999) 2075–2084.
[9] M. Tabei, T.D. Mast, R.C. Waag, A *k*-space method for coupled first-order acoustic propagation equations, *Journal of the Acoustical Society of America* 111 (2002) 53–63.
[10] Q.H. Liu, J. Tao, The perfectly matched layer for acoustics waves in absorptive media, *Journal of the Acoustical Society of America* 102 (1997) 2072–2084.
[11] A. Bermúdez, *Continuum Thermomechanics. Progress in Mathematical Physics*, Birkhauser-Verlag, Berlin, 2005.
[12] A.J. Berkhout, *Applied Seismic Wave Theory*, Elsevier, Amsterdam, 1987, pp. 109–110.
[13] W.C. Chew, W.H. Weedon, A 3D perfectly matched medium from modified Maxwell's equations with stretched coordinates, *Microwave Optical Technology Letters* 7 (1994) 599–604.
[14] M. Zampolli, A. Tesei, F.B. Jensen, N. Malm, J.B. Blottman, A computationally efficient finite element model with perfectly matched layers applied to scattering from axially symmetric objects, *Journal of the Acoustical Society of America* 122 (2007) 1472–1485.
[15] I. Singer, E. Turkel, A perfectly matched layer for the Helmholtz equation in a semi-infinite strip, *Journal of Computational Physics* 201 (2004) 439–465.
[16] H. Thorsten, F. Schmidt, L. Zschiedrich, Solving time harmonic scattering problems based on the pole condition, *SIAM Journal on Mathematical Analysis* 35 (2003) 547–560.
[17] D. Komatitsch, J. Tromp, A perfectly matched layer absorbing boundary condition for the second-order seismic wave equation, *Geophysical Journal International* 154 (2003) 146–153.
[18] A. Bermúdez, L. Hervella-Nieto, A. Prieto, R. Rodríguez, An optimal perfectly matched layer with unbounded absorbing function for time-harmonic acoustic scattering problems, *Journal of Computational Physics* 223 (2007) 469–488.